Copper(II)-benzotriazole coordination compounds in click chemistry: a diagnostic reactivity study

Article (Accepted Version)

Copper(II)-benzotriazole coordination compounds in click chemistry: A diagnostic reactivity study

Edward Loukopoulos,[a] Alaa Abdul-Sada,[a] Gizella Csire,[b] Csilla Kállay,[c] Adam Brookfield,[d] Graham J. Tizzard,[e] Simon J. Coles,[e] Ioannis N. Lykakis*[f] and George E. Kostakis*[a]

[a] Department of Chemistry, School of Life Sciences, University of Sussex, Brighton BN1 9QJ, UK. E-mail: G.Kostakis@sussex.ac.uk

[b] Department of Inorganic and Analytical Chemistry, University of Debrecen, H-4032 Debrecen, Hungary.

[c] MTA-DE Redox and Homogeneous Catalytic Reaction Mechanisms Research Group, University of Debrecen, H-4032 Debrecen, Hungary

[d] School of Chemistry, The University of Manchester, Manchester M13 9PL, UK.

[e] UK National Crystallography Service, Chemistry, University of Southampton SO1 71BJ, U.K

[f] Department of Chemistry, Aristotle University of Thessaloniki, Thessaloniki 54124, Greece. lykakis@chem.auth.gr

ABSTRACT

This diagnostic study aims to shed light on the catalytic activity of a library of Cu(II) based coordination compounds with benzotriazole-based ligands. We report herein the synthesis and characterization of five new coordination compounds formulated $[Cu^{II}(L^4)(MeCN)_2(CF_3SO_3)_2]$ (**1**), $[Cu^{II}(L^5)_2(CF_3SO_3)_2]$ (**2**), $[Cu^{II}(L^6)_2(MeCN)(CF_3SO_3)]\cdot(CF_3SO_3)$ (**3**), $[Cu^{II}(L^6)_2(H_2O)(CF_3SO_3)]\cdot(CF_3SO_3)\cdot 2(Me_2CO)$ (**4**), $[Cu^{I}_4(L^1)_2(L^{1'})_2(CF_3SO_3)_2]_2\cdot 4(CF_3SO_3)\cdot 8(Me_2CO)$ (**5**), derived from similar nitrogen-based ligands. The homogeneous catalytic activity of these compounds along with our previously reported coordination compounds (**6** -**13**), derived from similar ligands, is tested against the well-known Cu(I)-catalysed azide-alkyne cycloaddition reaction. The optimal catalyst

$[Cu^{II}(L^1)_2(CF_3SO_3)_2]$ (**10**) activates the reaction to afford 1,4-disubstituted 1,2,3-triazoles with yields up to 98% and without requiring a reducing agent. Various control experiments are performed to optimize the method as well as examine parameters such as ligand variation, metal coordination geometry and environment, in order to elucidate the behaviour of the catalytic system.

Introduction

In the constant search for efficient activation and optimization of organic reactions with transition metal elements, copper remains one of the most attractive options due to many advantages.[1–3] Apart from its abundance and low cost, copper presents an incredibly versatile chemistry and may be easily available in one of multiple (Cu^0, Cu^I, Cu^{II}, Cu^{III}) oxidation states. As a result, its salts and compounds can be powerful catalysts for reactions that involve both one and two-electron (radical and bond-forming) mechanisms. Furthermore, it can easily coordinate to heteroatoms as well as π-bonds to form organometallic intermediates that are crucial promoters of these transformations.

The Huisgen 1,3-dipolar cycloaddition[4,5] of organic azides and alkynes is a characteristic reaction in which the above principles are in full effect. In the absence of a catalyst, the reaction proceeds very slowly and under harsh conditions to produce a mixture of 1,4- and 1,5-disubstituted 1,2,3-triazoles with no regioselectivity (Scheme 1, pathway A). However, the introduction of a Cu^I source, as found independently by the groups of Meldal[6] and Sharpless[7], greatly improves the rate[8] and regioselectivity of the reaction to produce only the 1,4-disubstituted analogue (Scheme 1, pathway B) under favourable conditions. The resulting triazoles have considerable applications in various biological activities, and as a result the Cu-catalysed azide–alkyne cycloaddition (CuAAC) reaction has been employed in the fields of drug discovery[9], biochemistry[10–13] and materials science[14].

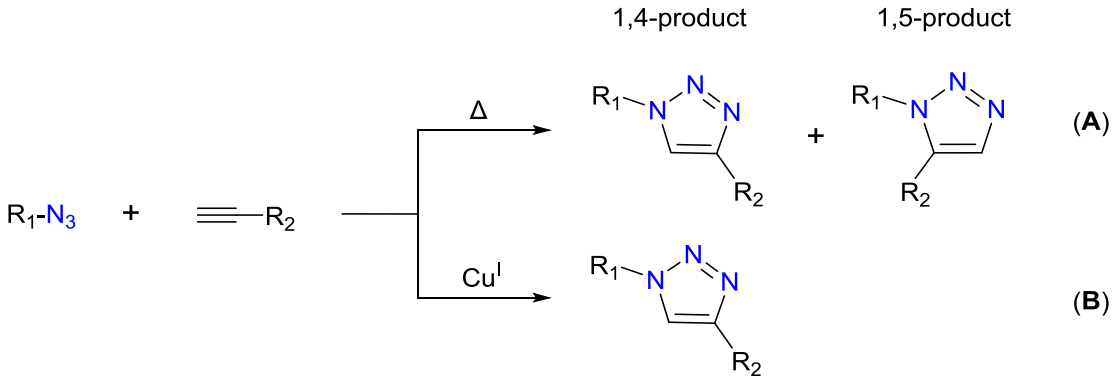

Scheme 1. General synthetic scheme of disubstituted 1,2,3-triazoles through azide-alkyne cycloaddition.

Multiple studies have shown that the reaction proceeds using almost any copper source as a catalytic precursor, as long as it generates catalytically active Cu^{I} species in the reaction medium[8,15–17]. The most popular method involves the use of an inexpensive Cu^{II} salt and a reducing agent (e.g sodium ascorbate[7] or hydrazine hydrate[18]) in large excess. The choice of the ligand is also important in the CuAAC reaction; it has been shown that certain nitrogen-containing ligands (e.g. amines[19], histidines[20], triazoles[21], benzimidazoles[22] and other polydentate chelators[13,23,24]) accelerate the transformation and enhance the stability of the Cu^{I} state through coordination, which protects the metal centres from oxidation. Therefore, the formation of unnecessary by-products is avoided.

In recent decades, there have been many attempts to bridge the fields of catalysis and coordination chemistry, in an effort to provide valuable information towards the mechanism of reactions as well as unveil the catalytic potential of coordination compounds. An important step has been the use of coordination polymers (CPs) and metal organic frameworks (MOFs)[25–27], low- or porous three-dimensional networks with possible catalytic activity[28–32]. A common strategy for the construction of neutral CPs involves the use of metal centres and protic bridging spacers, such as polycarboxylic ligands[33–35], to generate the framework and complete the charge balance. Another synthetic strategy incorporates neutral bridging ligands, mainly

nitrogen-based (e.g. derivatives of bipyridine[36], pyrazine[37,38], triazole[39–41], imidazole[41–44]) along with metal centres to afford cationic CPs. Focusing on the latter approach, we recently embarked in a series of studies that investigated the coordination and catalytic capabilities of coordination compounds based, mainly, on the semi-rigid benzotriazole-based organic ligand L^1 and its derivatives L^2 and L^3 (Scheme 2). Our first effort included isoskeletal Cu^{II} compounds that were found to promote the one pot synthesis of N-substituted dihydropyridines, from azines and ethyl propiolate, in methanol[45]. Through fine tuning we then isolated additional derivatives of this catalytic system and tested them against the synthesis of propargylic amines through the A^3 coupling[46] as well as in the multicomponent synthesis of poly-substituted pyrroles from aldehydes and nitrostyrenes[47], in alcoholic media. Various results from these studies indicate the formation of a Cu^I intermediate during the reaction, which acts as the catalytically active species. However, more specific details on the mechanistic nature of the catalyst remained yet elusive to us.

Having all these in mind, in this work we performed a study with a two-fold character. Firstly, to evaluate the efficacy of the catalysts derived from the benzotriazole-based organic ligand L^1 against other isotypical nitrogen-based ligands L^2 - L^7 (Scheme 2), such as substituted benzotriazoles (L^1-L^4 and L^7), benzimidazole (L^5) or imidazole (L^6), in a given reaction system. Secondly, to shed light on the mechanistic aspects and performance of the present catalytic library in the CuAAC reaction, a well-refined and known transformation that is promoted exclusively by Cu^I sources. To perform this diagnostic study, we herein report the synthesis and characterization of five new compounds formulated as $[Cu^{II}(L^4)(MeCN)_2(CF_3SO_3)_2]$ (**1**), $[Cu^{II}(L^5)_2(CF_3SO_3)_2]$ (**2**), $[Cu^{II}(L^6)_2(MeCN)(CF_3SO_3)]\cdot(CF_3SO_3)$ (**3**), $[Cu^{II}(L^6)_2(H_2O)(CF_3SO_3)]\cdot(CF_3SO_3)\cdot2(Me_2CO)$ (**4**), $[Cu^I_4(L^1)_2(L^{1'})_2(CF_3SO_3)_2]_2\cdot4(CF_3SO_3)\cdot8(Me_2CO)$ (**5**). We also report the catalytic performance of **1**-**5** in the one pot synthesis of 1,4-disubstituted 1,2,3-triazoles (click reaction).

The tested methods employ either organic halides or phenylboronic acid as starting materials, along with sodium azide to generate the organic azides *in situ* and avoid the isolation of potentially unstable intermediates. We additionally evaluate the respective catalytic performance of several suitable coordination compounds formulated as $[Cu^{II}(L^1)_2(MeCN)_2]\cdot 2(ClO_4)\cdot MeCN$ (**6**), $[Zn^{II}(L^1)_2(H_2O)_2]\cdot 2(ClO_4)\cdot 2MeCN$ (**7**), $[Cu^{I}(L^1)Cl]$ (**8**), $[Cu^{II}(L^1)_2(MeCN)_2]\cdot 2(BF_4)$ (**9**), $[Cu^{II}(L^1)_2(CF_3SO_3)_2]$ (**10**), $[Zn^{II}(L^1)_2(MeCN)_2]\cdot 2(CF_3SO_3)$ (**11**), $[Cu^{II}_2(L^2)_4(H_2O)_2]\cdot 4(CF_3SO_3)\cdot 4Me_2CO$ (**12**) and $[Cu^{II}_2(L^3)_4(CF_3SO_3)_2]\cdot 2(CF_3SO_3)\cdot Me_2CO$ (**13**) from our previously reported works, to provide further comparisons and draw useful conclusions towards our targets.

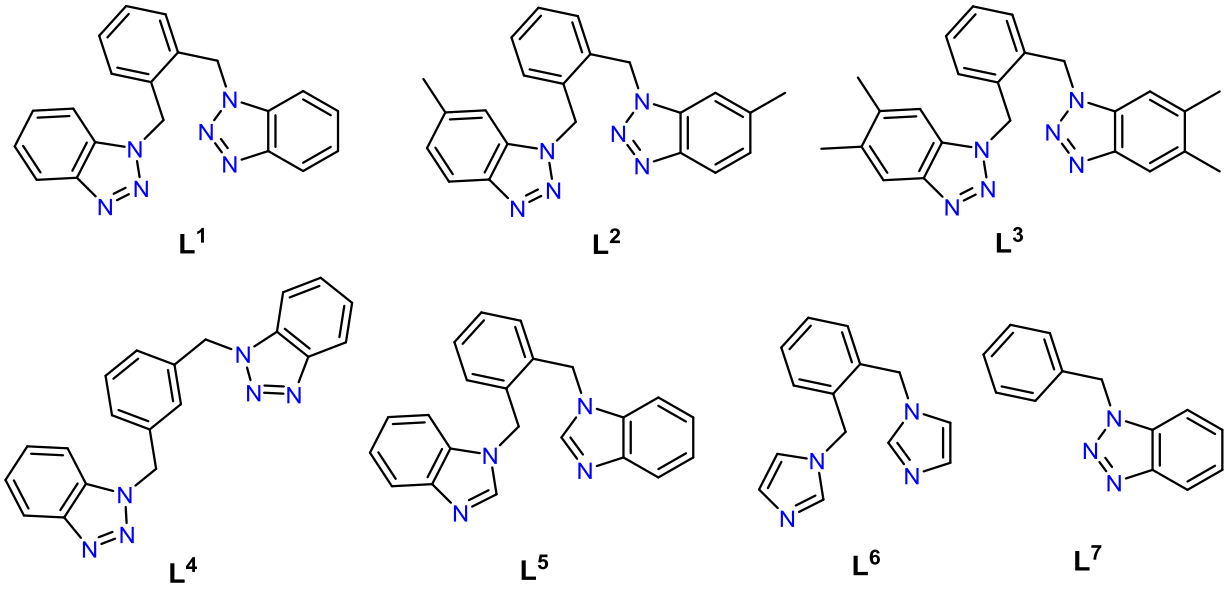

Scheme 2. The organic ligands (L^1-L^7) used in this study.

EXPERIMENTAL

Materials. Chemicals (reagent grade) were purchased from Sigma Aldrich, Acros Organics and Alfa Aesar. Materials and solvents were used with no further purification. Unless stated in their chemical formula, the metal salts used were anhydrous. Ligands L^1-L^4, L^7 and compounds **6-13** were synthesized according to the reported procedures[45,46,48]. Colourless block crystals of L^1, L^6 and L^7 [49] were also obtained; the relevant crystallographic parameters may be found in

the Supporting Information (Table S1). *Safety note*: Azides are potentially explosive; such compounds should be used in small quantities and handled with caution and the appropriate protection measures at all times.

Instrumentation. IR spectra of the samples were recorded over the range of 4000-600 cm^{-1} on a Perkin Elmer Spectrum One FT-IR spectrometer fitted with a UATR polarization accessory. EI-MS was performed on a VG Autospec Fissions instrument (EI at 70 eV). TGA analysis was performed on a TA Instruments Q-50 model (TA, Surrey, UK) under nitrogen and at a scan rate of 10°C/min. NMR spectra were measured on a Varian VNMRS solution-state spectrometer at 30°C. Chemical shifts are quoted in parts per million (ppm). Coupling constants (J) are recorded in Hertz (Hz).

EPR Spectroscopy. 9 GHz continuous-wave X-band electron paramagnetic resonance (EPR) spectra were recorded on a Bruker Biospin EMX spectrometer with a Bruker ER4119HS resonator. The spectra were obtained with 2.2mW microwave power and 2G modulation under non-saturating conditions at 5K. Low temperature measurements were achieved using an Oxford Instruments ESR900 cryostat. The Easyspin[50] software package was used for all simulations.

Cyclic voltammetry. The cyclic voltammograms of the Cu^{II} complexes were obtained by means of a Metrohm VA 746 Trace Analyzer equipped with a 747 VA Stand driven by a common PC. All the measurements were carried out in DMF and DMSO (0.10 M TBAP was used as the supporting electrolyte). Argon gas was bubbled through the complex solutions again to ensure the absence of oxygen. In each case, the voltammogram of the ligand was registered and no peaks were found. The systems were analysed at 25°C with a three electrode assembly. During the experiments, the working electrode was glassy carbon (glassy carbon electrode: CHI104). The reference electrode was a Vycor tip Ag/AgCl electrode stored in 3 M NaCl (BASI Instr. RE-5B, MF-2079), while the counter electrode was a platinum electrode

(distributed by ALS Co., Japan). The concentration of the complexes was $1 \cdot 10^{-3}$ M and the volume of the sample was 1 mL. Before each scan, the working electrode was treated with alumina paste (0.1 micron ordered from Buehler Company) and the surface was cleaned with the help of sandpaper. The electrochemical measuring system was calibrated with the $[Fe(CN)_6]^{3-}/[Fe(CN)_6]^{4-}$ redox system. The redox potential was 0.462 V, which is in good agreement with the published redox potential (0.458 V[51]). The potential range was changed between +800 and –1200 mV. The voltammograms were recorded at 25, 100, 1000 mV/s sweep rates. For the analysis of the voltammograms, we used the CACYVO program that was provided by the distributor of the instrument. The half-wave potential ($E_{1/2}$) values were calculated based on the following equation:

$E_{1/2} = \frac{E_{pc} + E_{pa}}{2}$, where E_{pc} and E_{pa} are the cathodic and anodic peak potentials, respectively.

Considering that $E_{1/2} = E^0$, the E^0 values throughout this work are referred to NHE, taking into account that $E^0_{Ag/AgCl}$ versus $E^0_{NHE\ (water)}$ is +209 mV at 25 °C.

$E^0 = E_{1/2} + E^0_{Ag/AgCl}$

X-Ray crystallography. Data for L^6, L^7, compounds **1**, **2** and triazoles **18aa** – **18ad** were collected (ω-scans) at the University of Sussex using an Agilent Xcalibur Eos Gemini Ultra diffractometer with CCD plate detector under a flow of nitrogen gas at 173(2) K and Cu Kα radiation (λ = 1.54184 Å). CRYSALIS CCD and RED software was used respectively for data collection and processing. Reflection intensities were corrected for absorption by the multi-scan method. Data for L^1 and compounds **3-5** were collected at the National Crystallography Service, University of Southampton.[52] All structures were determined using Olex2[53], solved using SHELXT[54,55] and refined with SHELXL-2014[56]. All non-H atoms were refined with anisotropic thermal parameters, and H-atoms were introduced at calculated positions and allowed to ride on their carrier atoms. Crystal data and structure refinement parameters for all compounds are given in Tables S1-S3. Geometric/crystallographic calculations were

performed using PLATON[57], Olex2[53], and WINGX[56] packages; graphics were prepared with Crystal Maker and MERCURY[58]. Each of the crystal structures has been deposited at the CCDC 1831783 – 1831794.

SYNTHETIC PROCEDURES

Synthesis of 1-(2-((1H-benzo[d]imidazol-1-yl)methyl)benzyl)-1H-benzo[d]imidazole (L^5). L^5 was synthesized according to the literature method[59] with slight modifications: To a solution of benzimidazole (3.0 g, 25 mmol) in DMF (50 ml) was added a solution of KOH (1.6 g, 25 mmol) in 20 ml H_2O. After 20 minutes of stirring, a,a'-dichloro-o-xylene (2.19 g, 12.5 mmol), was added slowly and the mixture was stirred under room temperature for 4 hrs. Then H_2O (30 mL) was added to the reaction mixture, and stirring was continued for another 1 hr. The mixture was then filtered to provide L^5 as a pale brown solid. Yield: 71% (2.98 g). ^{1}H NMR (500 MHz, $CDCl_3$) δ 7.84 (d, *J* = 8.0 Hz, 2H), 7.77 (s, 2H), 7.35 – 7.21 (m, 6H), 7.12 (d, *J* = 8.0 Hz, 2H), 7.06 – 7.03 (m, 2H), 5.28 (s, 4H). ^{13}C NMR (126 MHz, $CDCl_3$) δ 143.8, 142.8, 133.7, 132.9, 129.4, 129.0, 123.5, 122.7, 120.7, 109.7, 46.3. Selected IR peaks (cm^{-1}): 3087 (w), 1615 (w), 1496 (m), 1458 (w), 1428 (w), 1402 (w), 1393 (w), 1385 (w), 1366 (w), 1317 (w), 1287 (m) 1265 (m), 1230 (w), 1201 (s), 1006 (w), 963 (w), 937 (w), 891 (m), 866 (w), 849 (w), 771 (m), 733 (s), 645 (w), 631 (w), 619 (m). HRMS for $C_{22}H_{19}N_4$ [M + H]: theor. 339.1604 m/z, found 339.1611 m/z.

Synthesis of 1-(2-((1H-imidazol-1-yl)methyl)benzyl)-1H-imidazole (L^6).

L^6 was synthesized according to the literature method[60] with slight modifications: a solution containing imidazole (3.16 g, 46.4 mmol) and α,α′-dichloro-o-xylene (0.78 g, 4.46 mmol) in methanol (50 mL) was heated under reflux for 20 hrs. After cooling, the solvent was evaporated to give a yellow syrup, which was then dissolved in 80 ml aqueous potassium carbonate (6.13 g). The resulting solution was left undisturbed to produce large crystals which were identified as $[L^6]\cdot 2H_2O$. Yield: 1.0 g (82%). ^{1}H NMR (500 MHz, $CDCl_3$) δ 7.43 (s, 2H), 7.36 (dd, *J* =

5.7, 3.4 Hz, 2H), 7.09 (s, 2H), 7.07 (dd, *J* = 5.7, 3.4 Hz, 2H), 6.78 (s, 2H), 5.01 (s, 4H). ^{13}C NMR (126 MHz, $CDCl_3$) δ 137.3, 133.7, 130.1, 129.4, 119.2, 117.7, 48.1. HRMS for $C_{14}H_{15}N_4$ [M + H]: theor. 239.1291 m/z, found 239.1290 m/z.

Synthesis of $[Cu^{II}(L^4)(MeCN)_2(CF_3SO_3)_2]$ (**1**)

0.05 mmol (0.017 g) of L^4 and 0.10 mmol (0.036 g) of $Cu(OTf)_2 \cdot H_2O$ were dissolved in 10 mL of MeCN while stirring to produce a green solution. After 10 min of stirring, the solution was stored in a glass vessel and heated at 95 °C for 18 h. After cooling down, the solution was subjected to Et_2O using the vapour diffusion technique. Green block crystals were produced after 3 days. Selected IR peaks (cm^{-1}): 3564 (w), 3512 (w), 1651 (w), 1455 (m), 1321 (m), 1283 (m), 1234 (w), 1172 (w), 1059 (s), 1020 (s), 954 (w), 880 (w), 794 (w), 758 (s), 748 (s), 672 w), 626 (w). Yield: 16% (based on Cu). Elemental analysis for $C_{26}H_{22}CuF_6N_8O_6S_2$: C 39.81, H 2.83, N 14.29; found C 39.96, H 2.82, N 14.38.

Synthesis of $[Cu^{II}(L^5)_2(CF_3SO_3)_2]$ (**2**)

0.06 mmol (0.022 g) of L^4 and 0.12 mmol (0.044 g) of $Cu(OTf)_2 \cdot H_2O$ were dissolved in 15 ml acetone while stirring to produce a dark green solution. Then the solution was filtrated and layered over n-hexane in a 1:2 ratio to produce small blue block crystals after 3 weeks. Selected IR peaks (cm^{-1}): 3351 (br), 3125 (w), 1616 (w), 1558 (w), 1519 (m), 1484 (w), 1465 (m), 1397 (w), 1241 (s), 1224 (s), 1175 (m), 1028 (s), 928 (w), 849 (w), 740 (s), 669 (m). Yield: 9% (based on Cu). Elemental analysis for $C_{46}H_{36}CuF_6N_8O_6S_2$: C 53.22, H 3.50, N 10.80; found C 53.36, H 3.42, N 10.83.

Synthesis of $[Cu^{II}(L^6)_2(MeCN)(CF_3SO_3)] \cdot (CF_3SO_3)$ (**3**)

A 10 ml solution of $Cu(OTf)_2 \cdot H_2O$ (0.072 g, 0.2 mmol) in MeCN was dropwise added to a 10 ml solution of L^5 (0.068 g, 0.2 mmol) in methanol. The resulting blue solution was filtered, then carefully layered over Et_2O in a 1:2 ratio to produce blue block crystals after 1 week. Selected IR peaks (cm^{-1}): 3462 (br), 3145 (m), 1659 (w), 1522 (m), 1459 (m), 1445 (w), 1258

(s), 1244 (m), 1226 (s), 1174 (w), 1109 (m), 1089 (m), 1032 (s), 947 (w), 868 (w), 857 (w), 838 (w), 774 (m), 759 (m), 729 (s), 687 (w), 661 (s), 634 (m), 625 (m). Yield: 24% (based on Cu). Elemental analysis for $C_{32}H_{31}CuF_6N_9O_6S_2$: C 43.73, H 3.56, N 14.35; found C 43.70, H 3.72, N 14.43.

Synthesis of $[Cu^{II}(L^6)_2(H_2O)(CF_3SO_3)]\cdot(CF_3SO_3)\cdot 2(Me_2CO)$ (**4**)

A 5 ml solution of L^5 (0.038 mg, 0.16 mmol) in acetone was layered on a 8 ml solution of $Cu(OTf)_2\cdot H_2O$ (0.029 g, 0.08 mmol) in H_2O. Purple needles were obtained after 5 days. Selected IR peaks (cm^{-1}): 3516 (w), 3444 (w), 3135 (w), 1611 (w), 1523 (m), 1461 (m), 1441 (w), 1277 (m), 1263 (m), 1244 (s), 1224 (s), 1155 (m), 1108 (m), 1090 (m), 1026 (s), 950 (m), 842 (w), 827 (w), 773 (w), 758 (w), 734 (s), 667 (m), 655 (m), 634 (s). Yield: 31% (based on Cu). Elemental analysis for $C_{36}H_{42}CuF_6N_8O_9S_2$: C 44.46, H 4.35, N 11.52; found C 42.00, H 3.35, N 12.91. This result corresponds to the loss of two Me_2CO molecules (calcd. C 42.08, H 3.43, N 13.08).

Synthesis of $[Cu^{I}_4(L^1)_2(L^{1'})_2(CF_3SO_3)_2]_2\cdot 4(CF_3SO_3)\cdot 8(Me_2CO)$ (**5**)

0.06 mmol (0.022 g) of L^1 and 0.12 mmol (0.045 g) of $Cu^{I}(MeCN)_4\cdot CF_3SO_3$ were dissolved in 17.5 ml acetone while stirring to produce a light yellow solution. Then the solution was filtrated and layered over Et_2O in a 1:2 ratio to produce small yellow block crystals after 2 days. Selected IR peaks (cm^{-1}): 3395 (br), 1608 (w), 1597 (w), 1499 (w), 1522 (m), 1457 (m), 1275 (m), 1223 (s), 1165 (m), 1026 (s), 869 (w), 743 (m), 634 (s). Yield: 41% (based on Cu). Elemental analysis for $C_{96}H_{88}Cu_4F_{12}N_{24}O_{16}S_4$: C 47.17, H 3.63, N 13.75; found C 46.89, H 3.08, N 14.71. This result corresponds to the loss of four acetone molecules (calcd. C 46.77, H 2.85, N 14.87).

General Catalytic Protocol. To a sealed tube containing 0.5 mmol of sodium azide (0.033 g) in 3 mL of ethanol, 0.5 mmol of organic halide or boronic acid, 0.5 mmol of alkyne and 5 mol% of the catalyst were added and the mixture was stirred at reflux for the appropriate time. After completion of the reaction, the slurry was filtered upon a short pad of silica (to withhold the

catalyst) and the filtrate was evaporated under vacuum. The resulting residue was then separated by column chromatography using silica gel and a mixture of hexane/EtOAc (5/1 ratio for triazoles **18aa** – **18ae**, **18ba** – **18be**, 10/1 ratio for triazoles **18ca** – **18cd**) as the eluent, to afford the corresponding triazole product in pure form.

RESULTS

Synthetic aspects. Due to the similar chemical nature and behaviour of ligands L^2-L^7 compared to the prototype L^1, we employed similar methods and techniques to generate frameworks that resemble the coordination geometry and environment of the main catalyst **10**[46]. As a result, all newly reported compounds were synthesized under aerobic conditions and analogous concentrations. The experiments were mainly conducted using acetonitrile or acetone as the main solvent, in order to i) provide satisfying solubility for all ligands and metal salts, ii) maintain the same synthetic method that were used during experiments with L^1, iii) enable us to engineer the resulting coordination environment through the coordinating (MeCN) or non-coordinating (Me_2CO) capabilities of the solvents. The main crystallization technique that was used for all compounds in order to provide high diffraction quality crystals was liquid or vapour diffusion. In regards to the secondary crystallization solvent, the non-coordinating solvents Et_2O and n-hexane proved to be the best choices; nevertheless H_2O (a coordinating solvent) also provided some success during the synthesis of **4** and allowed us to slightly manipulate the coordination environment of Cu^{II}. Room temperature conditions were employed in almost all compounds, with the exception of **1**; it has been reported[48] that the temperature effect on L^4 further promotes the formation and dimensionality of coordination polymers. For this reason, the mixture in this case was initially heated at 95 °C. All compounds are soluble in DMF, less soluble in other common organic solvents (eg. acetonitrile, methanol, THF) and insoluble in water.

Crystal structure description. The crystal structures of compounds **6** – **13** have already been reported and described[45,46]. Hence, only the structures of **1** – **5** will be discussed in detail in this section. A summarizing table providing structural details for all compounds is given in Table 1. Since compound **10** serves as the main catalyst and reference point in this study, a brief description of its structural characteristics will also be included, prefacing the newly reported compounds. The reference catalyst **10** was synthesized using the benzotriazole-based L^1 ligand; the compound crystallizes in the triclinic $P\bar{1}$ space group and its asymmetric unit contains a Cu^{II} centre, one L^1 molecule and one triflate anion molecule. Due to the generated symmetry, the structure propagates into a ribbon-like one-dimensional framework with small cavities (Figure 1, left). The flexibility of the $–CH_2$ groups in L^1 allow for a coordination mode in which the planes of the benzotriazole molecules are found at an angle of 118.44(7)° to each other. Due to this, the metal centres are fairly separated and the corresponding Cu-Cu distance was measured at 9.0095(3) Å. Each Cu^{II} centre is coordinated to a total of six atoms and possesses an octahedral geometry through a $\{N_4O_2\}$ coordination environment. The axial positions of the octahedron are occupied by triflate oxygen atoms as the four nitrogen atoms from L^1 molecules in the equatorial positions create an almost perfect square plane. The mean Cu-O distance was measured at 2.536(4) Å, while the Cu-N bond lengths are 2.009(5) and 2.013(7) Å. No strong hydrogen bonds or other supramolecular interactions are observed. In addition, **10** has very similar structural characteristics (coordination geometry of the Cu centre and coordination mode of the ligand) to compound **2**, which utilized the benzimidazole-based ligand L^5, containing an identical 1D framework with small pores (Figure 1, right). For this reason, its structure will not be discussed further.

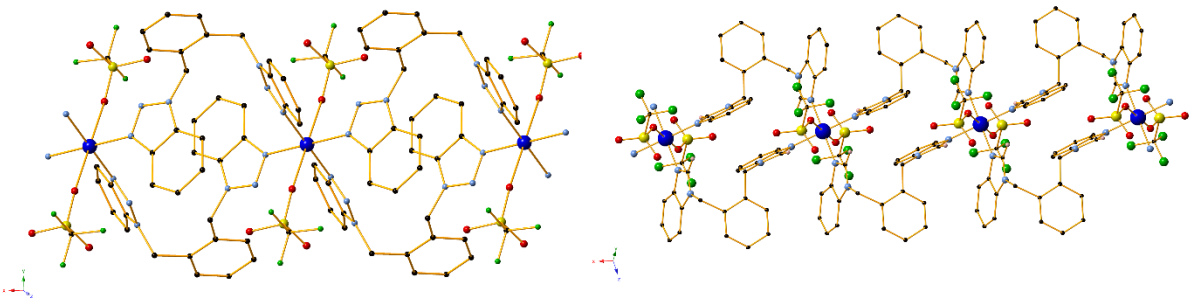

Figure 1. Part of the one-dimensional framework in compounds **10** (left) and **2** (right). The two complexes are isostructural. Certain H atoms are omitted for clarity. Colour code Cu (blue), C (black), H (light pink), N (light blue), O (red), S (yellow), F (light green).

1 was prepared using the L^4 ligand and crystallizes in the triclinic $P\bar{1}$ space group. One Cu^{II} centre, one L^4 molecule, two coordinating triflate anion molecules and two coordinating acetonitrile molecules are contained in the asymmetric unit. The L^4 ligand molecules in the structure adopt a type of *syn*- conformation that promotes the formation of a one-dimensional chain as shown in Figure 2. The behaviour of the flexible unit of L^4 is similar to the one of L^1, with an angle of 123.96(4)° between the planes of the benzotriazole moieties. However, due to the meta-substitution in L^4 the resulting polymer in **1** shows a Cu-Cu distance of 9.3801(5) Å, larger compared to **10**. Each Cu^{II} centre possesses a slightly distorted octahedral geometry and a $\{N_4O_2\}$ coordination environment in which the axial positions of the octahedron are occupied by the triflate oxygen atoms; relevant Cu-O distances were measured at 2.370(4) and 2.401(4) Å. The remaining four nitrogen atoms form a near-perfect square plane, as the mean Cu-N distances range from 1.994(5) to 2.003(4) Å. While similar coordination characteristics were found in the main catalyst **10**, in this case only two of the four nitrogen atoms that form the square plane derive from ligand molecules. The relevant N-Cu-N angles were found to be in the range of 87.82(15) to 91.16(17)°. Finally, no $\pi\cdots\pi$ interactions or strong hydrogen bonds were observed in the compound.

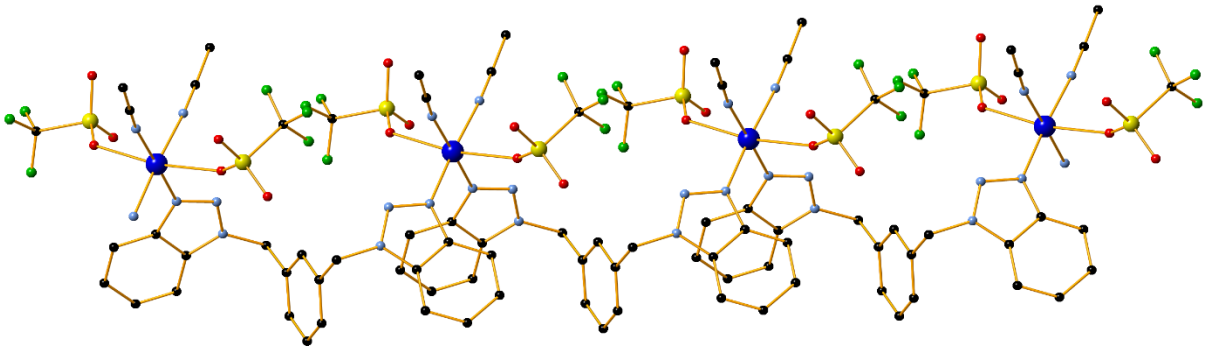

Figure 2. Part of the one-dimensional chain in **1**. H atoms are omitted for clarity. Colour code Cu (blue), C (black), N (light blue), O (red), S (yellow), F (light green).

The imidazole-based L^6 ligand was employed for the construction of compound **3**. The complex crystallizes in the monoclinic C2/c space group and its asymmetric unit contains one Cu^{II} centre, two L^6 molecules, two triflate anion molecules and one acetonitrile molecule. As in the cases of the benzotriazole (**10**) and benzimidazole (**2**) analogues, the Cu^{II} centres possess an octahedral geometry that also includes a $\{N_4\}$ square plane with ligand-deriving nitrogen atoms at distances ranging from 1.996(4) to 2.017(4) Å. As a result, **3** exhibits a similar one-dimensional framework as shown in Figure 3 (top). A triflate and an acetonitrile molecule also coordinate through the axial positions in significantly larger distances (Cu-O: 2.513(5) Å, Cu-N: 2.549(6) Å respectively) to complete the octahedron, while a second triflate anion is also present in the crystal lattice to account for the charge balance. In this case the distance between the metal centres was measured at 9.7264(3) Å, which is the highest relevant in the study. This may be attributed to the absence of the bulky phenyl groups which limits potential steric effects and the possible formation of weak C-H···π interactions. As a result of this increased flexibility, the angles between the planes of the imidazole moieties were measured at 100.1(2) and 111.5(3)°, differing significantly compared to the previous compounds.

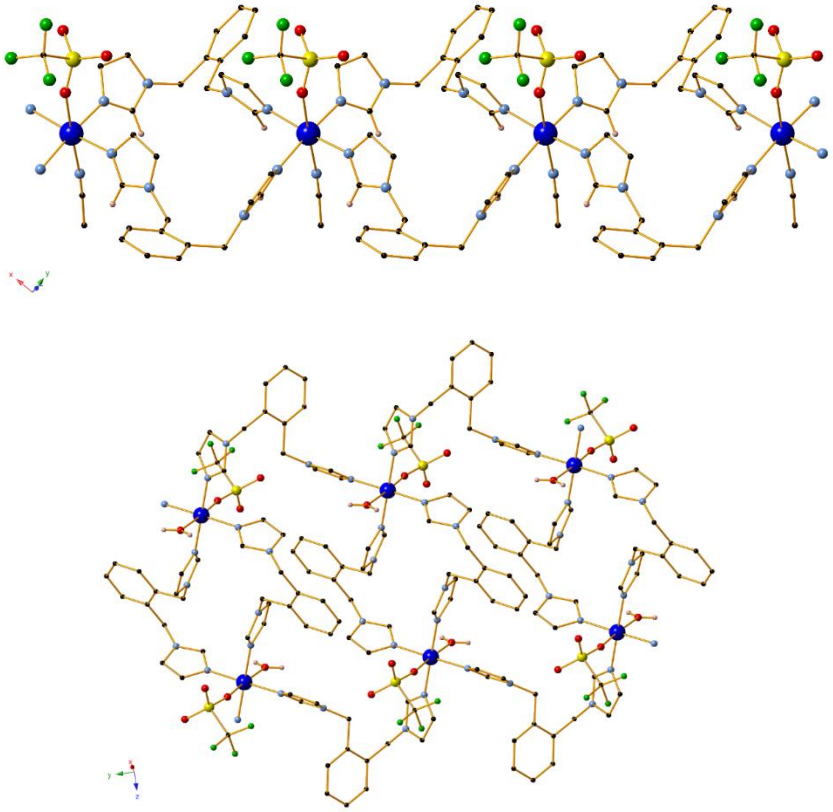

Figure 3. The one-dimensional frameworks in **3** (top) and **4** (bottom). Certain H atoms are omitted for clarity. Colour code Cu (blue), C (black), H (light pink), N (light blue), O (red), S (yellow), F (light green).

Compound **4** was also synthesized using L^6 and $Cu(OTf)_2 \cdot H_2O$ as the metal salt. Compared to **3**, compound **4** reveals an analogous one-dimensional framework which consists of the same $[Cu^{II}(L^6)_2(solvent)(CF_3SO_3)]$ units, however with some structural differences based on the use of different crystallization solvents (H_2O/Me_2CO instead of MeCN). In this case, the complex crystallizes in the monoclinic $P2_1/n$ space group and a water molecule acts as the coordinating solvent (Figure 3, bottom). This accounts for octahedral Cu^{II} centres with $\{N_4O_2\}$ environment, slightly different compared to the case of compound **3**, however the ligand-derived $\{N_4\}$ square plane is present on both occasions. A second triflate anion along with solvent molecules are also found in the crystal lattice. The structure of **4** is further stabilized by the formation of two

strong O-H···O hydrogen bonds between the oxygen from the water molecule and an oxygen atom of either a triflate anion or a solvent molecule in each case.

Determination of the structure of **5** by X-ray crystallography reveals a zero-dimensional Cu^{I} tetramer (Figure 4) which crystallizes in the triclinic space group $P\bar{1}$. All of the metal centres in this Cu_4 unit appear aligned in a single plane. Four organic ligands derived from L^1 are also present. An interesting case of ligand isomerism is observed in two of these ligands, as the -CH_2 linker is bonded to the central N atom of one of the benzotriazole moieties, generating the 1,2-disubstituted benzotriazole analogue ($L^{1'}$) despite the fact that pure crystals of L^1 were used during the synthesis. This phenomenon is common in substituted benzotriazole derivatives, as multiple studies by Katritzky's group[61,62] have shown that both the benzotriazol-1-yl and -2-yl adducts exist in solution; the position of this equilibrium has been found to be strongly dependant on parameters such as the polarity of the solvent, the temperature or the bulkiness of the substrate[63–67], however the 1-yl adduct remains predominant, which explains the presence of both species in the structure. Two triflate molecules are also present in these tetramer units, each coordinating to one metal centre. All Cu^{I} centres exhibit tetrahedral geometry; the two external centres have a $\{N_3O\}$ coordination environment which involves nitrogen atoms from three different ligand molecules (two as L^1 and one as $L^{1'}$). Respective Cu-N distances for these atoms were measured from 1.981(3) to 2.010(3) Å. The remaining metal centres in-between are coordinated to nitrogen atoms from two as L^1 and two $L^{1'}$ ligands, possessing an $\{N_4\}$ environment. In this case, the measured Cu-N distances were found to be slightly larger, ranging from 2.037(3) to 2.080(3) Å. In regards to the triflate coordination, the analogous Cu-O distance was calculated at 2.173(3) Å. Finally, the relevant angles for all tetrahedra were found to be in the range of 99.47(12) and 112.74(12)°.

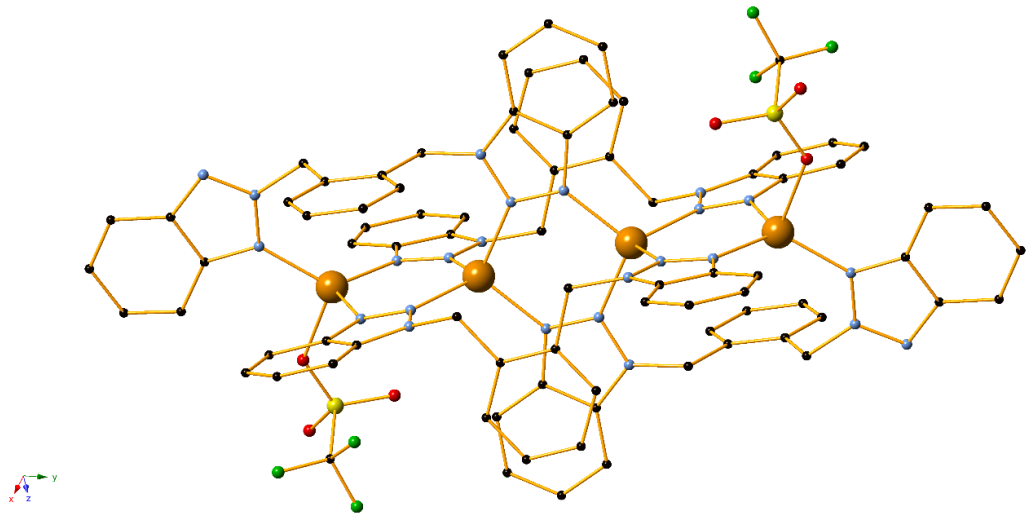

Figure 4. The structure of the tetrameric units in compound **5**. Lattice solvent and anion molecules, as well as H atoms are omitted for clarity. Colour code Cu (orange), C (black), N (light blue), O (red), S (yellow), F (light green).

Table 1. Structural summary of compounds **1-13**.

Entry	Compound	Ligand	Coordination Environment (M = Cu/Zn)	M source	Dimensionality
1	**1**	L^4	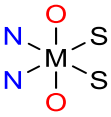	$Cu(OTf)_2 \cdot H_2O$	1D
2	**2**	L^5	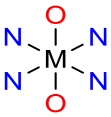	$Cu(OTf)_2 \cdot H_2O$	1D
3	**3**	L^6	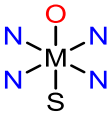	$Cu(OTf)_2 \cdot H_2O$	1D
4	**4**	L^6	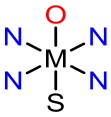	$Cu(OTf)_2 \cdot H_2O$	1D
5	**5**	L^1 , $L^{1'}$	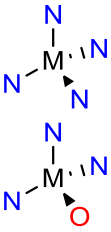	$Cu(OTf)_2 \cdot H_2O$	0D (tetramer)
6	**6**	L^1	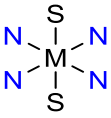	$Cu(ClO_4)_2 \cdot 6H_2O$	1D
7	**7**	L^1	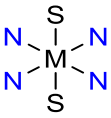	$Zn(ClO_4)_2 \cdot 6H_2O$	1D
8	**8**	L^1	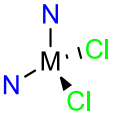	$Cu(ClO_4)_2 \cdot 6H_2O$	1D
9	**9**	L^1	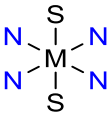	$Cu(BF_4)_2 \cdot 6H_2O$	1D
10	**10**	L^1	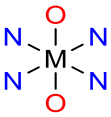	$Cu(OTf)_2 \cdot H_2O$	1D
11	**11**	L^1	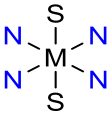	$Zn(OTf)_2$	1D
12	**12**	L^2	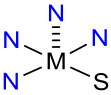	$Cu(OTf)_2 \cdot H_2O$	0D (dimer)
13	**13**	L^3	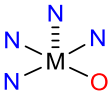	$Cu(OTf)_2 \cdot H_2O$	0D (dimer)

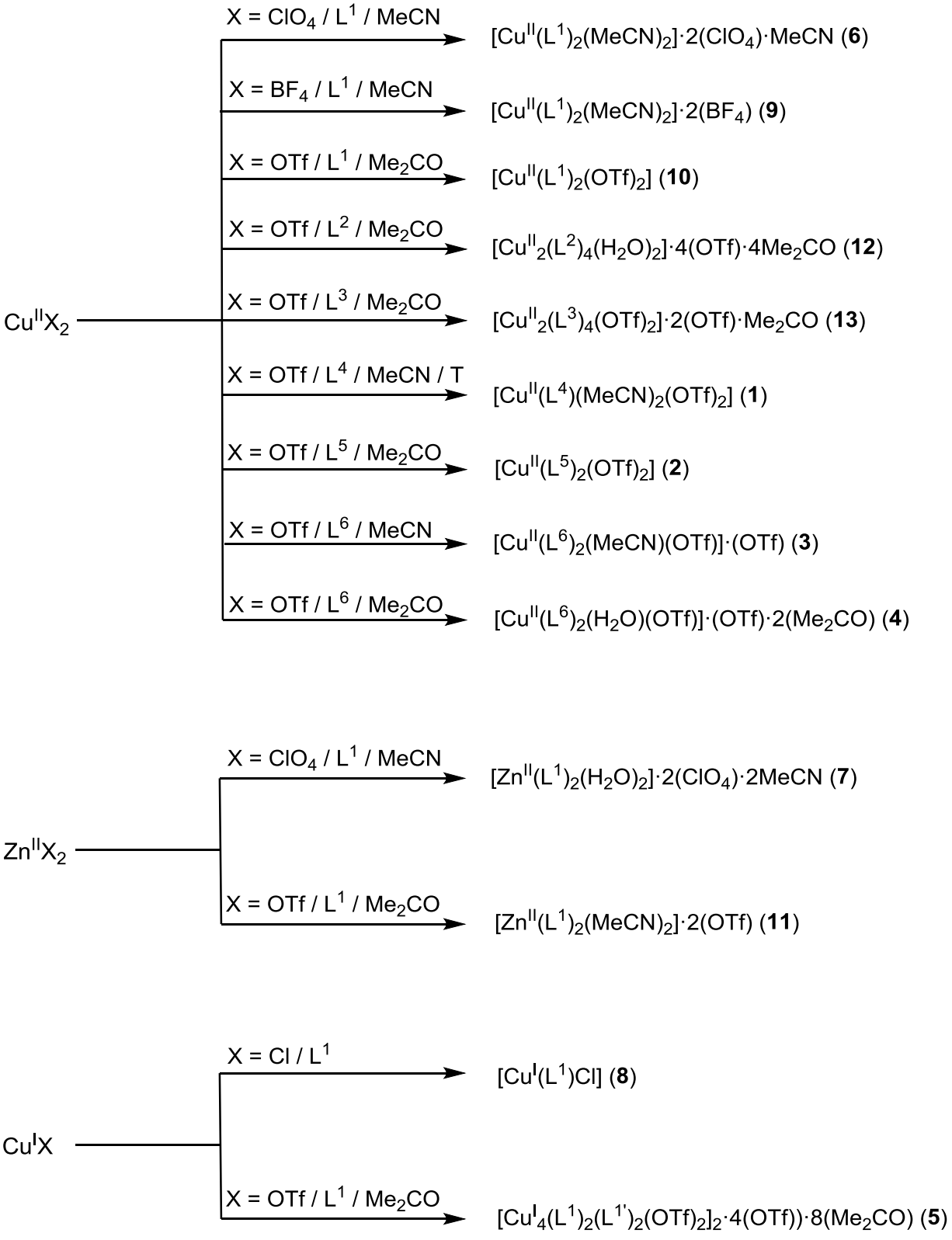

Scheme 3. A Schematic presentation of the synthesis of compounds **1**-**13**

Characterization of compounds.

We initially investigated the thermal stability of **1-5** through thermogravimetric analysis (TGA) experiments up to a temperature of 1000°C. The measurements revealed that the polymeric compounds **1-4** are slightly more stable than the zero-dimensional tetrameric complex **5**; the former retain their main metal-ligand core until the region of 260-300°C after which gradual decomposition to copper oxide begins. In complex **5**, the same procedure occurs at a slightly lower temperature region (~240°C). The TGA graphs are presented and interpreted in detail in the Supporting Information (Figures S29-S33).

ESI-MS (positive-ion mode) in methanolic solution for complexes **1-5** shows a variety of peaks depending on their behaviour in solution as well as the ligand used. The most common peaks can be found in all or almost all compounds and correspond perfectly to the respective $[Cu(L)]^+$, $[Cu(L)_2]^+$, $[Cu(L)(CF_3SO_3)]^+$ and $[Cu(L)_2(CF_3SO_3)]^+$ fragments. Additional peaks are also observed in each spectrum, which are consistent to various metal–ligand-anion fragments. For example, **1** and **2** also contain peaks that correspond to the respective $[Cu_2(L)_2(CF_3SO_3)_3]^+$ and $[Cu_2(L)_3(CF_3SO_3)_3]^+$ fragments. Imidazole-based compounds **3** and **4** present additional peaks that match the theoretical values for the $[Cu(L)_3]^+$ and $[Cu(L)_3(CF_3SO_3)]^+$ fragments. Finally, the ESI-MS spectrum of **5** reveals five main peaks which are attributed to the corresponding $[Cu(L)]^+$, $[Cu(L)_2]^+$, $[Cu(L)_2(CF_3SO_3)]^+$, $[Cu_2(L)_2(CF_3SO_3)]^+$ and $[Cu_2(L)_3(CF_3SO_3)]^+$ fragments. Overall, **1-5** appear to behave in solution similarly to the already reported compounds **6-13**. All ESI-MS spectra, along with a detailed analysis of the fragments, are presented in Figures S24–S28.

Catalytic studies. In order to provide an ideal scheme for the reaction we focused on the catalytic synthesis, which would avoid the isolation of the potentially unstable organic azides (especially azides with low molecular weights[15]). For these reasons, we adopted the multicomponent reaction between organic halides, alkynes and sodium azide as our initial

reaction scheme, in which the respective organic azide is generated *in situ*. The initial testing catalytic protocol included the use of benzyl chloride, sodium azide and phenylacetylene, as well as compound **10** as the homogeneous catalyst. After several catalytic tests (Table 2), it was found that optimal results were obtained when the reaction takes place in ethanol for 24 hrs, under reflux and 5 mol% of the catalyst (Table 2, entry 2). Under these conditions, the starting material is consumed and the reaction leads to the corresponding triazole **18aa** in 93% yield. To our delight, this result was obtained in the absence of any external reducing agent, providing substantial evidence towards the formation of a Cu^{I} intermediate during the reaction.

Table 2. Optimization of the synthesis of triazole **18aa** using **10** as the catalyst.

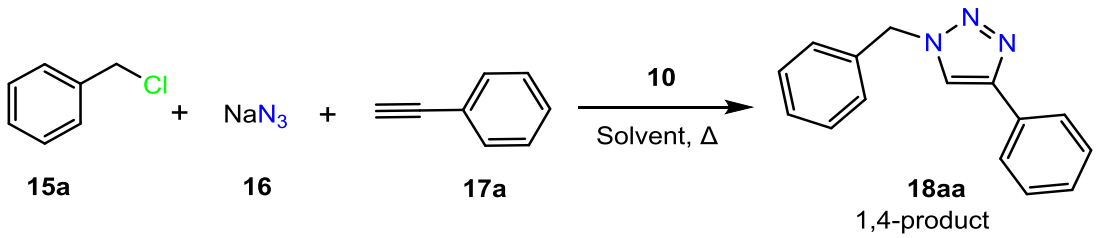

Entry	Solvent	Temperature (°C)	Time (h)	Loading (mol %)	Conversion (%)[a]	Yield (%)[b]	Regioselectivity 1,4/1,5-product	TON/TOF (hr^{-1})
1	MeOH	64	24	5	76	62	83:17	12.4/0.52
2	EtOH	78	24	5	100	93	99:1	18.6/0.78
3	iPrOH	82	24	5	94	76	98:2	15.2/0.63
4	MeCN	82	24	5	65	43	99:1	8.6/0.36
5	Toluene	110	24	5	NR	-	-	-
6	DMF	120	24	5	96	46	98:2	9.2/0.38
7	1,4-Dioxane	101	24	5	NR	-	-	-
8	H_2O	100	24	5	NR	-	-	-
9	EtOH	78	24	2.5	83	47	99:1	18.8/0.78
10	EtOH	78	1	5	45	22	98:2	4.4/4.4
11[c]	EtOH	78	24	5	93	82	97:3	16.4/0.68

12[d]	EtOH	78	24	5	87	87	99:1	17.4/0.73
13[e]	EtOH	78	24	5	100	93	99:1	18.6/0.78
14[e]	EtOH	78	1	5	99	92	99:1	18.4/18.4
15	EtOH	rt	24	5	NR	-	-	-

Reaction conditions: benzyl chloride (0.5 mmol), sodium azide (0.5 mmol), phenylacetylene (0.5 mmol), **10**, solvent (3 mL). [a]: based on benzyl chloride, [b]: calculated from the crude mixture by ^{1}HNMR. [c]: with 0.5 ml solvent. [d] with the addition of 15% $P(Ph)_3$. [e] with the addition of 15% Sodium Ascorbate. NR = no reaction. The reported[68] ^{1}HNMR peaks of the 1,5-analogue were employed to determine regioselectivity.

Encouraged by this result, we then compared the performance of various Cu^{I} and Cu^{II} salts under the same reaction conditions (Table S5) which demonstrated the better performance of **10**. In addition; in some of these cases, the starting material was not even entirely consumed.

Having obtained the optimal conditions for our system, we then tested a number of substrates in order to study the catalytic scope and limitations of **10**. Initial substrate screening included the use of organic halides as starting materials as well as a variety of terminal alkynes (e.g. aromatic, alkyl, linear, containing hydroxyl or carboxylate groups). The results are presented in Scheme 4. The reaction affords triazoles in excellent (88 - 99%) yields when aromatic or substituted aliphatic alkynes are used. In regards to the organic halide, increasing the strength of the leaving group from Cl^{-} (entries **18aa** – **18af**) to Br^{-} (entries **18ba** – **18be**) led to improved results as expected. It is also worth noting that the triazoles derived from benzyl halide proved to be very easy to crystallize. As such, X-Ray crystallography structures of representative triazoles **18aa** – **18ad** are additionally included. Iodobenzene was also tested as a possible substrate in our attempts to generate the relevant aryl triazole analogues, however these efforts were unsuccessful. This was not surprising as the azidonation of aryl halides[21,69,70] is generally a slow process that requires very harsh or tedious conditions. We therefore

employed the inexpensive and readily available benzeneboronic acid in order to obtain the corresponding product[71]. To our delight, the resulting triazole **18ca** was generated in a very good 80% yield, as seen in Scheme 5. Additional screening of the arylboronic acid with other alkynes led to the formation of triazoles **18cb** – **18cd** in poorer yields, whereas reactions with 2-hydroxyphenylboronic acid did not yield any product (**18ce** – **18cf**). Nevertheless, these results provided us with another potential pathway for our catalyst which avoids the isolation of unstable organic azide intermediates.

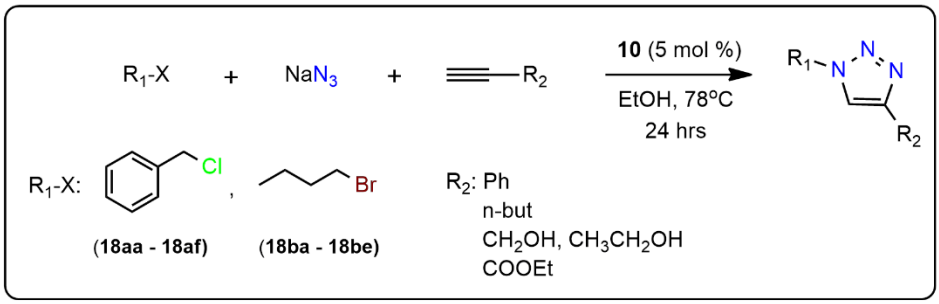

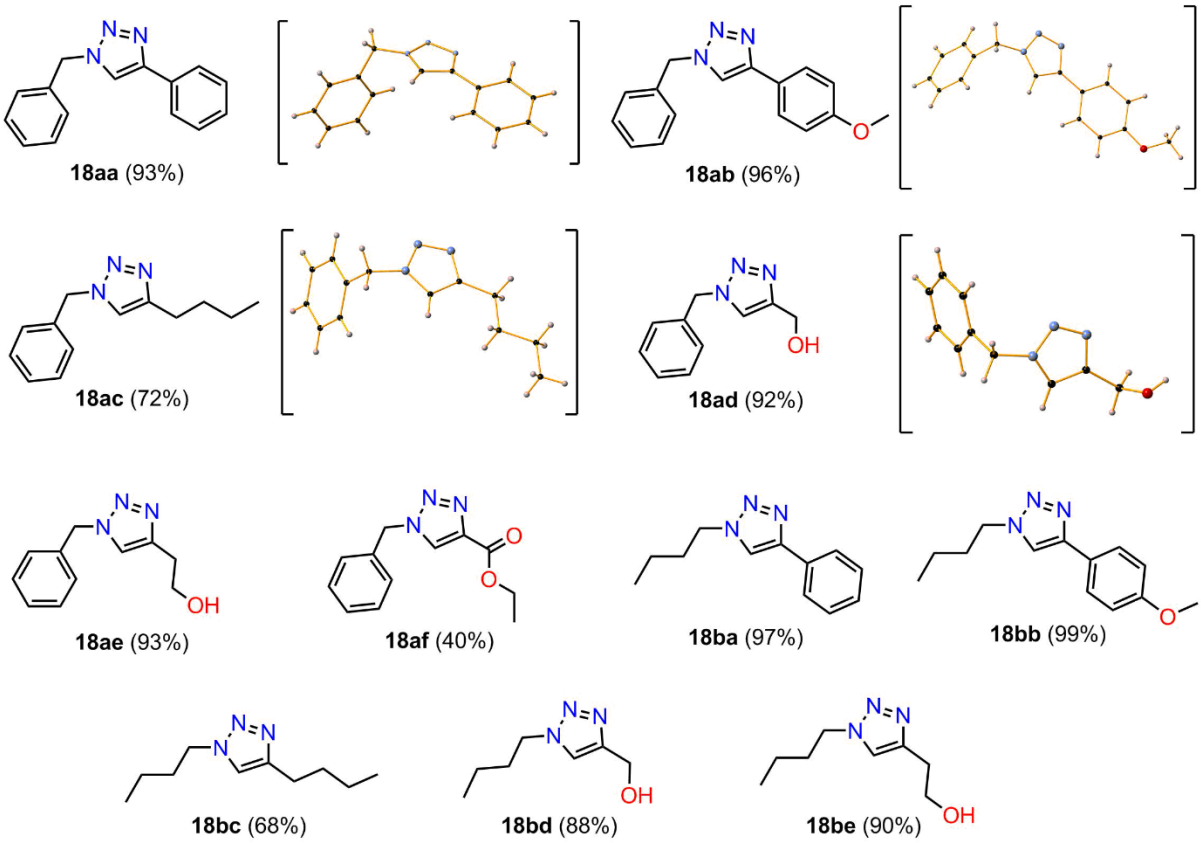

Scheme 4. Catalytic activity of **10** in the multicomponent synthesis of 1,4-disubstituted 1,2,3-triazoles from organic halides.

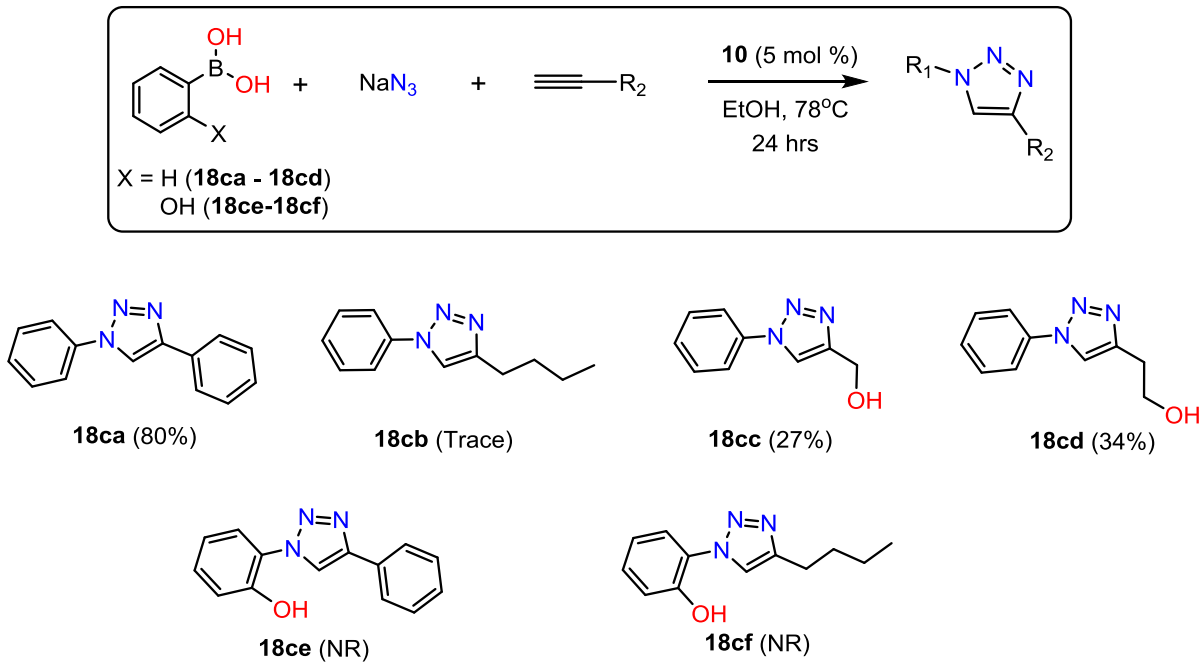

Scheme 5. Catalytic activity of **10** in the one-pot synthesis of 1-aryl-1,2,3-triazoles from boronic acid.

Cyclic Voltammetry studies. As a first step, we performed cyclic voltammetric studies of the ligands L^1, L^2, L^5, L^6. During this process, we neither did not observe any processes in the negative nor in the positive potential range and only the CV of the TBAP was measurable. Therefore, we could establish that the ligands are stable in DMSO and in DMF and they are not oxidized. We then performed the CV studies for the Cu based compounds (Figures 5 and 6). Compounds **2**, **10** and **12** were selected for these purposes due to their structural characteristics and catalytic performance. **2** and **10** can be reduced in the first step and can be then oxidized back in the second step in the positive potential range. The I_a/I_c is ~1 and the $v^{1/2}$-|Ic| function is not linear whereas the potential difference of the anodic and cathodic peak potential is more than 59 mV indicating a structural change. This can be rationalized to the different coordination preference of the Copper element in different oxidation states (I or II),

therefore the intra-conversion (II to I to II) takes place in a slower manner, or the electron crossing may be slower on the electrode surface. These results show that these processes are quasi-reversible. The redox potentials are positive in both cases and substantially different when compared with the redox potential of $Cu(NO_3)_2$, thus supporting that the measured potential values correspond to Cu(II) complexes. The CV of compound **12** complex is similar to the $Cu(NO_3)_2$ cyclic voltammogram in both solvents, indicating that compound **12**, despite having similar structural characteristics with **2** and **10**, is not stable in DMF and in DMSO.

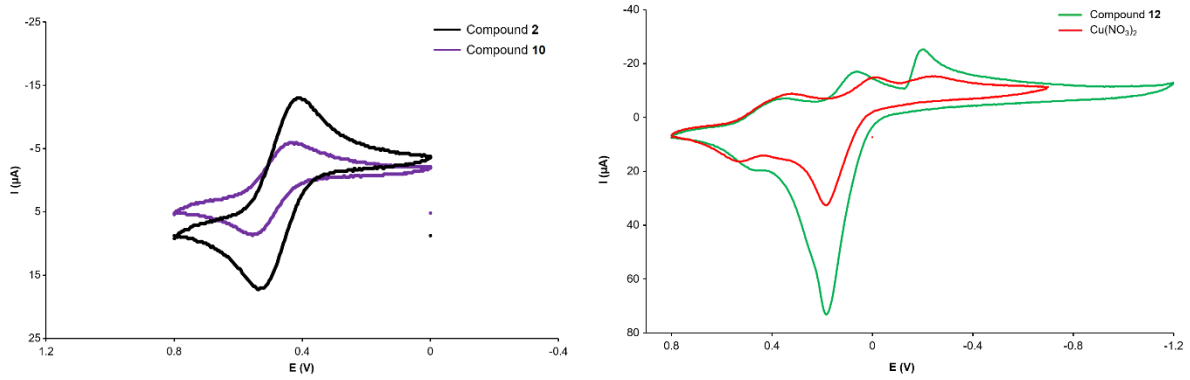

Figure 5. Voltammograms of **2** (black) and **10** (purple) in 0.1 M TBAP/DMF (Potential range: 800-0 mV. Scan rate 100 mV/s). (right) Voltammograms of **12** (green) and $Cu(NO_3)_2$ (red) in 0.1 M TBAP/DMF (Potential range: 800-(-1200) mV for **12**, 800-(-700) mV for $Cu(NO_3)_2$. Scan rate 100 mV/s).

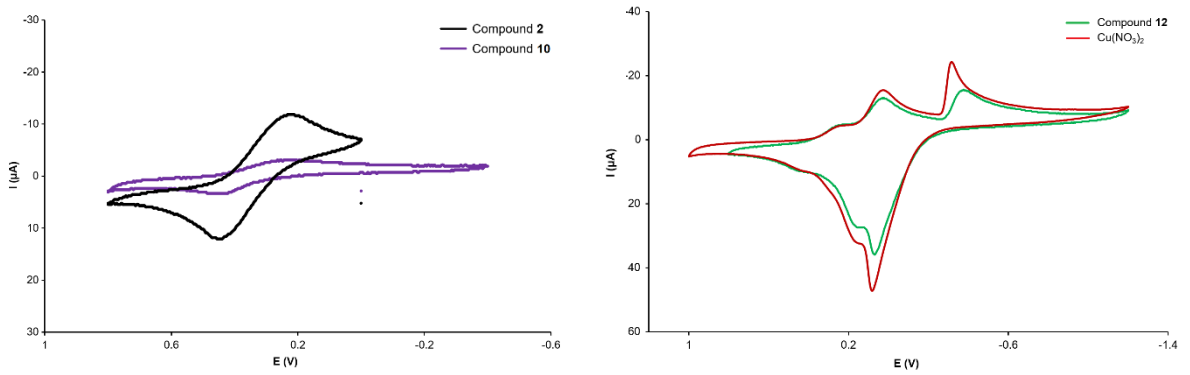

Figure 6. (left) Voltammograms of **2** (black) and **10** (purple) in 0.1 M TBAP/DMSO (Potential range: 800-0 mV for **2**, 800-(-400) mV for **10**. Scan rate 100 mV/s). (right) Voltammograms

of **12** (green) and $Cu(NO_3)_2$ (red) in 0.1 M TBAP/DMSO (Potential range: 800-(-1200) mV for **12**, 1000-(-1200) mV for $Cu(NO_3)_2$. Scan rate 100 mV/s).

EPR Studies. To gain further structural insights, X-band EPR studies of characteristic compounds **2, 10, 12** were performed. The spectra of polycrystalline samples in solid-state or in frozen alcoholic solution were recorded at a temperature of 5K. For compound **2**, a comparison between the spectra of the solid-state sample and the one in frozen methanol (Figure S35, right) shows similar signals in both case, however fewer hyperfine lines are observed in the former. A closer look at the crystallographic parameters of the compound reveals severe axial distortion in the octahedron due to Jahn-Teller effects, with the Cu-N and Cu-O distances at 2.022(3) and 2.549(3) Å respectively. Furthermore, a series of weak intramolecular interactions (C–H···π, C–H···O_{OTf}) involving the –CH group of the imidazole moiety is observed. Both these phenomena contribute to weaker magnetic coupling between neighbouring cations and eventually a narrowing of the hyperfine lines. The best simulation (Figure S35, left) was obtained with (g_x, g_y, g_z) = (1.92, 1.99, 2.3) ± 0.01 and A = 200 ± 30 MHz which is in agreement with the above observations. In contrast, the EPR signal of **2** in methanolic solution provides much more defined hyperfine lines which are consistent to a Cu^{II} (S=1/2) interaction with four ^{14}N nuclei from L^5 ligands in a square planar environment, pointing to an eventual $\{N_4O_2\}$ octahedral geometry. A plausible hypothesis for the difference in the clarity of the two spectra could be that, in solution, methanol molecules replace the triflate anions and coordinate to the Cu^{II} centres, removing any potential formation of C–H···O interactions[72,73].

Similar studies for compound **10**, as can be seen in Figure S36, show that Cu^{II} retains the $\{N_4O_2\}$ octahedral geometry in alcoholic solution, and the structure remains polymeric. This result is consistent with previously conducted[46] UV-Vis studies which showed that the

compound retains a similar coordination environment in solution. It is worth noting that the spectrum in this case is very well defined compared to the one of compound **2**, as no weak C–H···O interactions are formed in the absence of the imidazolic moiety. A comparison of the hyperfine lines shows slight changes in the coordination environment upon solvation but does not alter, indicating once again potential replacement of the triflate anions with ethanol molecules. A simulation with very good agreement for the polycrystalline sample at room temperature provided the fitting parameters (g_x, g_y, g_z) = (2.08852, 2.03142, 2.29635) ± 0.01 and A = 520 ± 30 MHz, indicating that the unpaired electron is localized in the $d_{x^2-y^2}$ orbital. Furthermore, they are in accordance to the corresponding values of similar Cu^{II} complexes with a $\{N_4O_2\}$ coordination environment[74–76].

While the crystallographic data for **12** could not be optimally refined, the Cu^{II} centres clearly exhibited a square pyramidal geometry in the crystal structure, with a $\{N_3O\}$ environment in the equatorial plane. The X-band EPR studies (Figure S37) of the polycrystalline sample at 5K further confirm this behaviour. Reasonable fits are obtained for (g_x, g_y, g_z) = (1.96, 2.04, 2.28) ± 0.01 and A = 350 ± 30 MHz; these values are in satisfying agreement to the ones of related Cu^{II} complexes with a $\{N_4O\}$ coordination sphere[77,78]. Once again, a narrowing of the hyperfine lines is also observed, possibly due to the formation of weak π···π and C–H···π interactions within the crystal structure.

Mechanistic studies

The aforementioned homogeneous catalytic performance of **10** in the azide-alkyne cycloaddition provides us with yet another organic transformation in which our library of 1D Cu^{II} CP catalysts may be applied. More importantly, the presence of a Cu^{I} source is necessitated for this specific reaction to occur; this serves as an excellent blueprint, which could shed light into the mechanistic function of our catalysts. Up to this point, we have established that our polymeric Cu^{II} compounds retain their nature in alcoholic solution, and can generate Cu^{I}

species when tested as pre-cursor catalysts in organic reactions under alcoholic media which involve the formation of the important copper-acetylide intermediate. We embarked in an extensive set of control experiments and techniques which could enable us to i) diagnose the exact nature of the generated Cu^{I} species, ii) find the limits of the present catalytic system, iii) identify the importance of the Cu^{II} pre-cursor in the catalytic activity, iv) further examine the effect of parameters such as ligand variation, metal effect, polymeric nature, dimensionality, geometry and coordination sphere.

Firstly, the importance of metal selection in the construction of the catalysts was evaluated. Zn^{II}-based compounds **7** and **11** were tested as catalysts for the synthesis of **18aa**, as they are isostructural to **10**, containing the same one-dimensional framework; they also behave similarly in solid and solution state. Recent investigations[79,80] on the feasibility of a ZnAAC system have shown that the reaction is indeed possible. Albeit it requires the presence of a reducing agent (none present in our proposed system) and is highly sensitive to steric effects in regards to the choice of alkyne. However, no product was formed in both cases (Table 4, entries 7 and 11). Given the inactivity of Zn centre towards the AAC reaction, this experiment excludes the possibility that the reaction is promoted by the ligand.

The next step was to assess the performance of Cu^{I} complexes from our backlog of related catalysts. Relevant compounds **5** and **8** were employed for these purposes, accounting for average yields as seen in Table 4, entries 5 and 8. This allowed us to narrow our fine-tuning efforts to Cu^{II} compounds. Therefore, we then opted to study the effect of the choice of metal ion during the catalytic process. The comparison tests in this case involved the isoskeletal 1D catalysts **6**, **9** and **10** (Table 4, entries 6, 9, 10) that differ in the counter anion (ClO_4^-, BF_4^-, OTf^- respectively). The results show significant differences in the afforded yield, with the OTf^- analogue exhibiting superior behaviour and the BF_4^- analogue accounting for the lowest activity. In addition, lower conversion (90%) of the starting material was observed in both

ClO_4^- and BF_4^- analogues. Furthermore, we have documented in previous studies that an anion conversion of ClO_4^- to Cl^- (in **6**) and BF_4^- to F^- (in **9**) is also taking place, inhibiting the catalytic performance.[45-46] These results indicate that $Cu(OTf)_2$ is the ideal choice of metal salt for the construction of our catalysts. Having also in mind that the triflate analogues provided the most encouraging results during the evaluation of Cu^I compounds and Cu^I/Cu^{II} salts (Table 1, entries 3 and 6), we envision that this performance is established as either the reaction requires the presence of a weak base to get a proton or the triflate unit has better resistance to the oxidation/reduction reaction, compared to ClO_4^- or BF_4^-. Moreover, any anion conversion issues that would inhibit the catalytic activity are avoided.

We then opted to examine the influence of the nitrogen-based ligand. The use of organic ligands L^2 and L^3 in which the benzotriazole moieties contain $–CH_3$ groups in positions 5 and 5,6 respectively resulted in the isolation of coordination compounds **12** and **13**. Both of these compounds show important structural differences compared to the reference catalyst **10** which derived from the parent ligand L^1. More specifically, the Cu^{II} centres possess different coordination geometry and the complexes have no polymeric nature, forming dicopper dimers instead. As seen in Table 4, entries 12 and 13, the catalytic tests for **12** and **13** showed average behaviour compared to **10**. This may be attributed to the aforementioned structural differences as well as a possible second sphere coordination effect to the Cu^{II} centres, due to the presence of the $–CH_2$ groups. We also employed the ligand 1,3-bis((1H-benzo[d][1,2,3]triazol-1-yl)methyl)benzene (L^4) to determine the effect of the position of the substituted benzotriazole molecules. Compared to the ortho-substitution in parent ligand L^1, the meta-substitution in L^4 provides increased flexibility to account for any potential steric effects. For this reason, the resulting 1D polymer **1** reveals larger Cu-Cu distances compared to **10** as well as larger angles between the benzotriazole molecules. **1** also provides increased space for substrate accommodation, as the four nitrogen atoms which comprise the square plane of the $\{N_4O_2\}$

coordination environment are derived from two L^4 and two MeCN molecules. However, its catalytic activity proved to be lower (Table 4, entry 1); we can thus conclude that this lack of ligand molecules leads to different and less active species during the catalysis, making **1** a less effective catalytic precursor. Having this result in mind, we focused exclusively on nitrogen-based ligands with 1,2-substitution. The use of benzimidazole (compound **2**) or imidazole (compounds **3**, **4**) instead of benzotriazole generates topological equivalent Cu^{II}-based 1D frameworks; however, their use as catalysts reveals a considerable decrease in the product yield (Table 4, entries 3, 4). As CV studies show that the benzimidazole-based analogue **2** behaves similarly to **10**, the yield difference can be attributed in electronic factors / second coordination sphere effect, as well as the absence of the bulky phenyl group in the case of the imidazole-based compounds. The possibility that more drastic species are formed with the benzotriazole ligand should also be considered. It is worth noting that both compounds **3** and **4** present the ligand-derived $\{N_4\}$ square plane that is required for the catalytic activity, however they have slight differences in the species that occupy the axial positions of the octahedron (OTf^-/MeCN versus OTf^-/H_2O). The latter parameter appears to have no effect in the catalytic performance, based on the similar yields measured in each case (69 and 70% respectively). Furthermore, to determine the importance of the polymeric nature for our catalysts, we employed the ligand 1-benzyl-1H-1,2,3-benzotriazole (L^7), as the mono-substituted version of L^1, to guarantee the generation of 0D coordination compounds. The *in situ* reaction of $Cu(OTf)_2$ and L^7 yields the corresponding product in poorer yields (Table 4, entry 14) indicating the necessity of a bis-substituted ligand. Finally, the *in situ* reaction of $Cu(OTf)_2$ and L^1 also resulted in significantly lower yield (Table 4, entry 15), showcasing that other, non-catalytically active species are formed during this process. From these results, we conclude that the well-characterized, polymeric precursors have higher catalytic efficacy.

In regards to the use of additives, it was found that the presence of sodium L-ascorbate enhances the Cu^{I} to Cu^{II} conversion (Table 3, entries 13 and 14), therefore improving the catalytic affinity. However, after 24 hours the catalytic conversion is similar to that without any additive. Triphenylphosphine (PPh_3) was also tested as an additive in the reaction; apart from its role as a reducing agent, PPh_3 may potentially react with the organic azide to eventually produce the corresponding amine through the Staudinger reaction[81], thus deactivating the CuAAC transformation. However, no significant effect in the yield was observed in our catalytic tests (Table 3, entry 12), indicating that PPh_3 is not involved in the catalytic cycle.

Additionally, a series of EPR experiments was performed monitoring the synthesis of triazole **18aa** using **10** as the catalyst, in order to investigate the nature of the copper-based compound during the reaction. A comparison of the afforded spectra during the first 120 minutes of the reaction, as shown in Figure S38, confirms the constant presence of Cu^{II} species in the solution, albeit with a continuous decrease in the intensity, which could indicate the change into EPR silent Cu^{I}. In comparison, similar studies were performed with the addition of the reducing agent sodium-L-ascorbate in the reaction mixture (Figure S38, right). While the intensity decrease is higher in the first 60 minutes of the reaction, the signals after 120 minutes are eventually similar to the ones without the presence of the additive, which is consistent to the similar catalytic results as previously mentioned.

Considering all these parameters and taking into account the above CV and EPR studies, we conclude to a possible mechanistic pathway depicted in Scheme 5. CV studies showed reversible transition $Cu^{II}(L^1)_2$ (**A**) to $Cu^{I}(L^1)_2$ (**B**) for compounds **2** and **10** but not for **12**, therefore we considered $Cu^{I}(L^1)_2$ (**B**) to be the possible catalytic active species. However, the comparison of the TOF values 4.4 (1 hour) and 0.8 (24 hours) (Table 2, entries 2 and 10) indicates structural change of the catalyst. The crystallographic characterization (as reported in previous studies)[45] of the 1D compound $[Cu^{I}(L^1)Cl]$ (**8**) as the deactivated catalytic specie,

confirms the partial dissociation of the ligand L yielding the $Cu^{I}(L^{1})$ (**C**) specie. The structure of **C** can be a 1D $[Cu^{I}N_2]$ compound, or due to the flexibility of the organic ligand it may consist of dimeric species. In these cases, the transition of **C** to the corresponding $Cu^{II}(L^{1})$ (**D**) cannot be excluded. EPR studies during the first 120 minutes of the reaction confirm the presence of Cu^{II} species in the solution, thus excluding the possibility that the Cu^{II} has converted in full to Cu^{I} at the beginning of the reaction. As the reaction proceeds, the excess of the produced 1,4-triazoles, that have similar coordination abilities to L^{1}, yields in further dissociation of L^{1} and formation of the species $[CuN_4]$ (**E**) and termination of the catalytic cycle. The two Cu^{I} units in the crystallographically characterized **C** are at an approximate distance of 8.74 Å, therefore any chance that the reaction is promoted from a dimeric specie[8,17] should be excluded for this catalytic system. Therefore, both active species **B** and **C** could catalyse the present 1,3-dipolar cycloaddition, as shown in Scheme 6. Consequently, a coordination of Cu to the acetylene takes place forming the corresponding Cu(I) acetylide intermediate, that in the presence of the azide undergoes a cyclization process through an unusual six-membered copper metallacycle intermediate. This pathway is supported by theoretical studies on copper-catalyzed 1,3-dipolar cycloaddition process and synthesis of azoles.[82,83] Finally, the ring contraction to a triazolyl-copper derivative is followed by protonolysis that delivers the triazole product and closes the catalytic cycle.

Table 4. Catalytic evaluation of compounds **1-13** in the synthesis of triazole **18aa**.

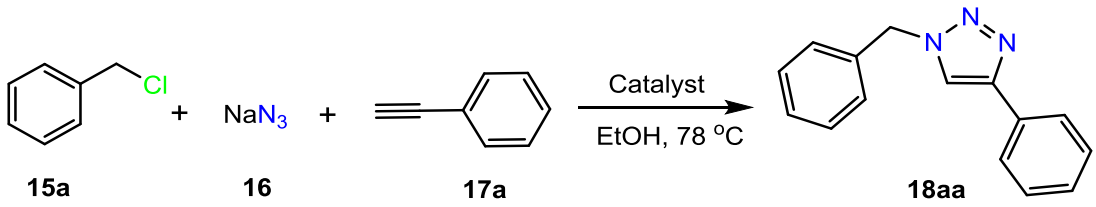

15a **16** **17a** **18aa**

Entry	Catalyst	Conversion (%)[a]	Yield (%)[b]	Regioselectivity of **18aa**[c]
1	**1**	99	74	99
2	**2**	99	84	99
3	**3**	100	69	99
4	**4**	100	70	99
5	**5**	99	77	99
6	**6**	90	56	99
7	**7**	NR	-	-
8	**8**	100	58	98
9	**9**	90	47	99
10	**10**	100	93	99
11	**11**	NR	-	-
12	**12**	97	78	98
13	**13**	94	76	98
14	$Cu(OTf)_2 \cdot H_2O$ + L^7	87	28	99
15	$Cu(OTf)_2 \cdot H_2O$ + L^1	99	57	99

(S = solvent. Reaction conditions: benzyl chloride (57.5 µL, 0.5 mmol), sodium azide (32.5 mg, 0.5 mmol), phenylacetylene (55 µL, 0.5 mmol), catalyst (5 mol %), EtOH (3 mL), heated at 78°C for 24 h. [a]: based on benzyl chloride, [b]: calculated from the crude mixture by ^{1}HNMR. [c]: calculated from regioisomers 1,4-product : 1,5-product.

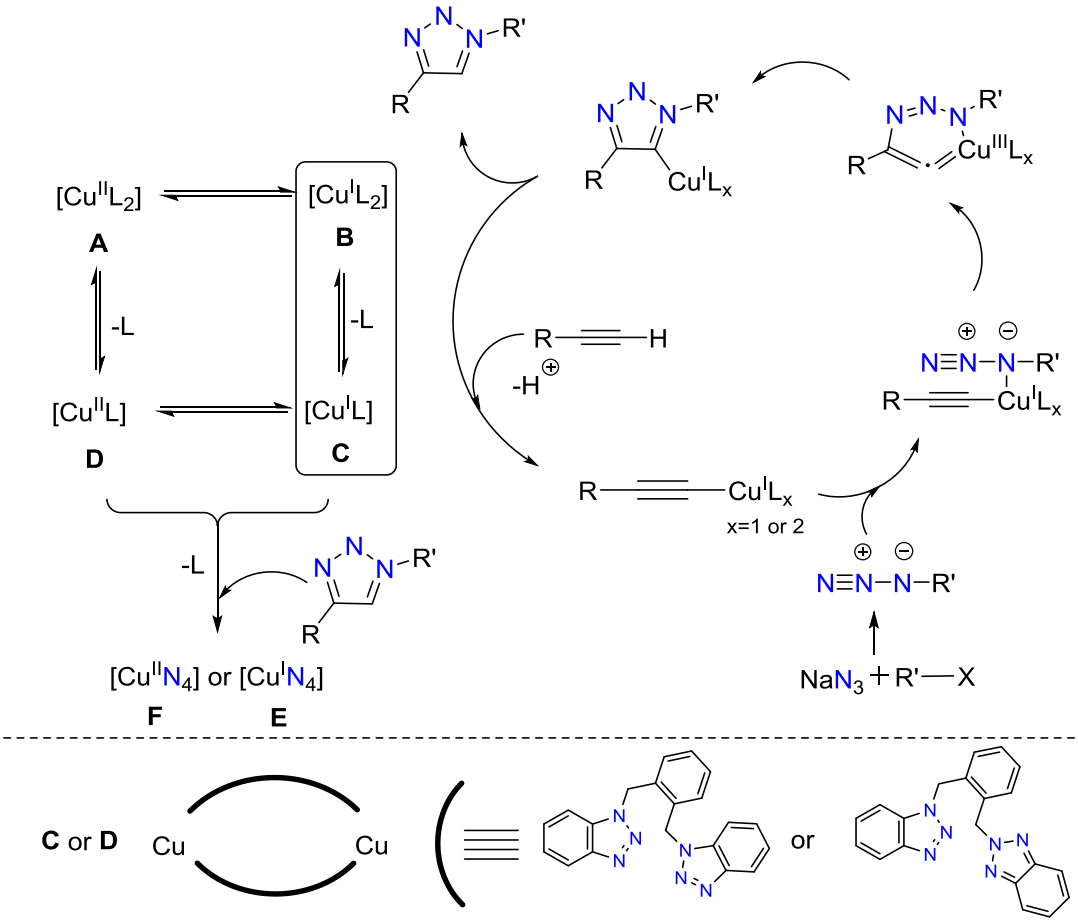

Scheme 6. A plausible mechanism of the AAC reaction catalysed by **10**.

CONCLUSIONS

In this work, we added a series of Cu coordination compounds with nitrogen-containing ligands in our pre-existing library of analogous catalysts and attempted to understand their homogeneous catalytic performance and mechanistic nature through their activity in the well-known Cu^{I} promoted AAC reaction. In particular, compound $[Cu^{II}(L^{1})_2(CF_3SO_3)_2]$ (**10**) is the optimal catalyst affording 1,4-disubstituted 1,2,3-triazoles with moderate to excellent (27-99%) yields without requiring a reducing agent. Furthermore, the proposed method avoids the isolation of potentially unstable organic azides, using either organic halides or benzeneboronic acid as starting materials.

CV studies in selected samples showed that fine-tuning the organic ligand has a significant effect on the electrochemical properties (**12** differs to **2** and **10**). The coordination

sphere of **2** and **10** is rather similar which is proved by the similar formal potential values. The measured formal potential values are more negative in DMSO than in DMF, which supports that it is much more difficult to reduce the complexes in stronger donor solvents. This fact may help us to choose the right solvent for a more effective catalysed reaction.

Through an extensive set of control experiments and techniques, we optimized and fine-tuned of our system. Our studies confirm that **10** can act as an excellent precursor in a number of organic reactions under alcoholic media[46] providing Cu^{I} active species. Initiating the catalysis from a polymeric Cu^{II} compound appears essential for the system, since our efforts to obtain the corresponding Cu^{I} derivatives or improve the catalytic performance with monomeric analogues were not successful. This diagnostic study enabled us to identify the benzotriazole-based ligand as the most suitable for our catalysts, as well as confirm the optimal metal geometry and coordination environment for the precursor. Furthermore, the semi-flexibility of the ligand through the introduction of the $–CH_2$ groups appears to be crucial, allowing for the formation and fine-tuning of the initial polymeric compounds, as well as the transformation to the various species during the catalytic cycle. Based on our extensive research with this system, we believe that the benzotriazole unit is an ideal N-donor and could be used as an excellent co-linker for the synthesis of suitable porous carboxylate-based mixed-ligand MOF compounds or oligomeric species towards catalytic redox reactions. At last, this study provides a wealth of information, which will help us explore the catalytic potential of other metals (e.g Co^{II}, Mn^{II}, Ag^{I}) with similar ligands. As such, our efforts will focus on this in the future.

Acknowledgements

We thank the EPSRC UK National Crystallography Service at the University of Southampton for the collection of the crystallographic data for L^1 and compounds **3**-**5**.[52] The EPSRC UK National Electron Paramagnetic Resonance Service at The University of Manchester is also

gratefully acknowledged. G.C. & C.K. acknowledge support from the ÚNKP-17-4 New National Excellence Program of the Ministry of Human Capacities.

References

1. X. Zhu and S. Chiba, *Chem. Soc. Rev.*, 2016, **45**, 4504–4523.
2. S. E. Allen, R. R. Walvoord, R. Padilla-Salinas, and M. C. Kozlowski, *Chem. Rev.*, 2013, **113**, 6234–6458.
3. S. D. McCann and S. S. Stahl, *Acc. Chem. Res.*, 2015, **48**, 1756–1766.
4. R. Huisgen, *Angew. Chemie Int. Ed. English*, 1963, **2**, 565–598.
5. R. Huisgen, *Angew. Chemie Int. Ed. English*, 1963, **2**, 633–645.
6. C. W. Tornøe, C. Christensen, and M. Meldal, *J. Org. Chem.*, 2002, **67**, 3057–3064.
7. V. V. Rostovtsev, L. G. Green, V. V. Fokin, and K. B. Sharpless, *Angew. Chemie - Int. Ed.*, 2002, **41**, 2596–2599.
8. M. Meldal and C. W. Tornøe, *Chem. Rev.*, 2008, **108**, 2952–3015.
9. P. Thirumurugan, D. Matosiuk, and K. Jozwiak, *Chem. Rev.*, 2013, **113**, 4905–4979.
10. R. L. Weller and S. R. Rajski, *Org. Lett.*, 2005, **7**, 2141–2144.
11. M. D. Best, *Biochemistry*, 2009, **48**, 6571–6584.
12. M. Yang, J. Li, and P. R. Chen, *Chem. Soc. Rev.*, 2014, **43**, 6511–6526.
13. M. Yang, A. S. Jalloh, W. Wei, J. Zhao, P. Wu, and P. R. Chen, *Nat. Commun.*, 2014, **5**, 4981.
14. W. Xi, T. F. Scott, C. J. Kloxin, and C. N. Bowman, *Adv. Funct. Mater.*, 2014, **24**, 2572–2590.
15. J. E. Hein and V. V. Fokin, *Chem. Soc. Rev.*, 2010, **39**, 1302.
16. E. Haldón, M. C. Nicasio, P. J. Pérez, P. J. Pérez, M. A. Pericàs, F. Maseras, M. C. Nicasio, P. J. Pérez, Y. Ji, J.-M. Vincent, H.-J. Youn, D. Y. Chi, and N. H. Hur, *Org. Biomol. Chem.*, 2015, **13**, 9528–9550.

17. L. Jin, D. R. Tolentino, M. Melaimi, and G. Bertrand, *Sci. Adv.*, 2015, **1**, 1–5.

18. A. Pathigoolla, R. P. Pola, and K. M. Sureshan, *Appl. Catal. A Gen.*, 2013, **453**, 151–158.

19. A. N. Semakin, D. P. Agababyan, S. Kim, S. Lee, A. Y. Sukhorukov, K. G. Fedina, J. Oh, and S. L. Ioffe, *Tetrahedron Lett.*, 2015, **56**, 6335–6339.

20. K. Tanaka, C. Kageyama, and K. Fukase, *Tetrahedron Lett.*, 2007, **48**, 6475–6479.

21. T. R. Chan, R. Hilgraf, K. B. Sharpless, and V. V. Fokin, *Org. Lett.*, 2004, **6**, 2853–2855.

22. V. O. Rodionov, S. I. Presolski, S. Gardinier, Y. H. Lim, and M. G. Finn, *J. Am. Chem. Soc.*, 2007, **129**, 12696–12704.

23. V. O. Rodionov, S. I. Presolski, D. D. Díaz, V. V. Fokin, and M. G. Finn, *J. Am. Chem. Soc.*, 2007, **129**, 12705–12712.

24. G. C. Kuang, H. A. Michaels, J. T. Simmons, R. J. Clark, and L. Zhu, *J. Org. Chem.*, 2010, **75**, 6540–6548.

25. S. R. Batten, N. R. Champness, X.-M. Chen, J. Garcia-Martinez, S. Kitagawa, L. Öhrström, M. O'Keeffe, M. P. Suh, and J. Reedijk, *CrystEngComm*, 2012, **14**, 3001.

26. S. R. Batten, N. R. Champness, X.-M. Chen, J. Garcia-Martinez, S. Kitagawa, L. Öhrström, M. O'Keeffe, M. Paik Suh, and J. Reedijk, *Pure Appl. Chem.*, 2013, **85**, 1715–1724.

27. S. R. Batten and N. R. Champness, *Phil. Trans. R. Soc.*, 2017, **375**, 1–4.

28. A. Corma, H. García, and F. X. Llabrés i Xamena, *Chem. Rev.*, 2010, **110**, 4606–55.

29. Z. Zhou, C. He, L. Yang, Y. Wang, T. Liu, and C. Duan, *ACS Catal.*, 2017, **7**, 2248–2256.

30. Z. Sun, J. Chen, and T. Tu, *Green Chem.*, 2017, **19**, 789–794.

31. X. Wang, M. Liu, Y. Wang, H. Fan, J. Wu, C. Huang, and H. Hou, *Inorg. Chem.*, 2017,

acs.inorgchem.7b02106.

32. Y.-B. Huang, J. Liang, X.-S. Wang, and R. Cao, *Chem. Soc. Rev.*, 2017, **46**, 126–157.

33. C. Falaise, J. Delille, C. Volkringer, H. Vezin, P. Rabu, and T. Loiseau, *Inorg. Chem.*, 2016, **55**, 10453–10466.

34. X. L. Wang, Y. Xiong, X. T. Sha, G. C. Liu, and H. Y. Lin, *Cryst. Growth Des.*, 2017, **17**, 483–496.

35. J. M. Seco, S. Pérez-Yáñez, D. Briones, J. Á. García, J. Cepeda, and A. Rodríguez-Diéguez, *Cryst. Growth Des.*, 2017, **17**, 3893–3906.

36. K. Biradha, M. Sarkar, and L. Rajput, *Chem. Commun.*, 2006, 4169–4179.

37. E. A. de Campos, N. J. O. Silva, F.-N. Shi, and J. Rocha, *CrystEngComm*, 2014, **16**, 10439–10444.

38. F. Y. Wardana, S. W. Ng, and A. C. Wibowo, *Cryst. Growth Des.*, 2015, **15**, 5930–5938.

39. Y. F. Peng, H. Y. Ge, B. Z. Li, B. L. Li, and Y. Zhang, *Cryst. Growth Des.*, 2006, **6**, 994–998.

40. A. X. Tian, J. Ying, J. Peng, J. Q. Sha, Z. G. Han, J. F. Ma, Z. M. Su, N. H. Hu, and H. Q. Jia, *Inorg. Chem.*, 2008, **47**, 3274–3283.

41. J.-L. Du, T.-L. Hu, S.-M. Zhang, Y.-F. Zeng, and X.-H. Bu, *CrystEngComm*, 2008, **10**, 1866.

42. J.-C. Geng, L. Qin, X. Du, S.-L. Xiao, and G.-H. Cui, *Zeitschrift für Anorg. und Allg. Chemie*, 2012, **638**, 1233–1238.

43. S. Samai and K. Biradha, *Cryst. Growth Des.*, 2011, **11**, 5723–5732.

44. S. Y. Hao, S. X. Hou, Z. C. Hao, and G. H. Cui, *Spectrochim. Acta - Part A Mol. Biomol. Spectrosc.*, 2018, **189**, 613–620.

45. M. Kallitsakis, E. Loukopoulos, A. Abdul-Sada, G. J. Tizzard, S. J. Coles, G. E. Kostakis, and I. N. Lykakis, *Adv. Synth. Catal.*, 2017, **359**, 138–145.

46. E. Loukopoulos, M. Kallitsakis, N. Tsoureas, A. Abdul-Sada, N. F. Chilton, I. N. Lykakis, and G. E. Kostakis, *Inorg. Chem.*, 2017, **56**, 4898–4910.

47. D. Andreou, M. Kallitsakis, E. Loukopoulos, C. Gabriel, G. E. Kostakis, and I. N. Lykakis, *J. Org. Chem.*, 2018, **83**, 2104–2113.

48. E. Loukopoulos, N. F. Chilton, A. Abdul-Sada, and G. E. Kostakis, *Cryst. Growth Des.*, 2017, **17**, 2718–2729.

49. P. Selvarathy Grace, S. R. Jebas, B. Ravindran Durai Nayagam, and D. Schollmeyer, *Acta Crystallogr. Sect. E Struct. Reports Online*, 2012, **68**, o1132–o1132.

50. S. Stoll and A. Schweiger, *J. Magn. Reson.*, 2006, **178**, 42–55.

51. I. M. Kolthoff and W. J. Tomsicek, *J. Phys. Chem.*, 1934, **39**, 945–954.

52. S. J. Coles and P. A. Gale, *Chem. Sci.*, 2012, **3**, 683–689.

53. O. V Dolomanov, A. J. Blake, N. R. Champness, and M. Schröder, *J. Appl. Crystallogr.*, 2003, **36**, 1283–1284.

54. G. M. Sheldrick, *Acta Crystallogr. Sect. A Found. Adv.*, 2015, **71**, 3–8.

55. G. M. Sheldrick, *Acta Crystallogr. Sect. A*, 2008, **64**, 112–122.

56. L. J. Farrugia, *J. Appl. Crystallogr.*, 1999, **32**, 837–838.

57. A. L. Spek, *J. Appl. Crystallogr.*, 2003, **36**, 7–13.

58. C. F. Macrae, P. R. Edgington, P. McCabe, E. Pidcock, G. P. Shields, R. Taylor, M. Towler, and J. Van De Streek, *J. Appl. Crystallogr.*, 2006, **39**, 453–457.

59. Z. Shi and R. P. Thummel, *J. Org. Chem.*, 1995, **60**, 5935–5945.

60. B. F. Hoskins, R. Robson, and D. A. Slizys, *J. Am. Chem. Soc.*, 1997, **119**, 2952–2953.

61. A. R. Katritzky, X. Lan, J. Z. Yang, and O. V. Denisko, *Chem. Rev.*, 1998, **98**, 409–548.

62. A. R. Katritzky, K. Yannakopoulou, E. Anders, J. Stevens, and M. Szafran, *J. Org. Chem.*, 1990, **55**, 5683–5687.

63. A. R. Katritzky, S. Perumal, and W.-Q. Fan, *J. Chem. Soc. Perkin Trans. 2*, 1990, 2059–

2062.

64. A. R. Katritzky, K. Yannakopoulou, W. Kuzmierkiewicz, J. M. Aurrecoechea, G. J. Palenik, A. E. Koziol, and M. Szczesniak, *J. Chem. Soc. Perkin Trans. I*, 1987, 2673–2679.

65. A. R. Katritzky, S. Rachwal, B. Rachwal, and J. W. Frankenfeld, *Int. J. Chem. Kinet.*, 1995, **27**, 351–357.

66. J. R. L. Smith and J. S. Sadd, *J. Chem. Soc. Perkin Trans. 1*, 1975, 1181–1184.

67. G. E. Kostakis, P. Xydias, E. Nordlander, and J. C. Plakatouras, *Inorg. Chim. Acta*, 2012, **383**, 327–331.

68. Y. C. Wang, Y. Y. Xie, H. E. Qu, H. S. Wang, Y. M. Pan, and F. P. Huang, *J. Org. Chem.*, 2014, **79**, 4463–4469.

69. W. Zhu and D. Ma, *Chem. Commun.*, 2004, 888.

70. A. R. Hajipour and F. Mohammadsaleh, *Tetrahedron Lett.*, 2014, **55**, 6799–6802.

71. C. Z. Tao, X. Cui, J. Li, A. X. Liu, L. Liu, and Q. X. Guo, *Tetrahedron Lett.*, 2007, **48**, 3525–3529.

72. W. Zhang, N. Saraei, H. Nie, J. R. Vaughn, A. S. Jones, M. S. Mashuta, R. M. Buchanan, and C. A. Grapperhaus, *Dalton Trans.*, 2016, **45**, 15791–15799.

73. R. Jain, T. J. Gibson, M. S. Mashuta, R. M. Buchanan, and C. A. Grapperhaus, *Dalton Trans.*, 2016, **45**, 18356–18364.

74. R. M. Krishna and S. K. Gupta, *Bull. Magn. Reson.*, 1994, **16**, 239–291.

75. C. Jubert, A. Mohamadou, J. Marrot, and J.-P. Barbier, *J. Chem. Soc. Dalt. Trans.*, 2001, 1230–1238.

76. Z. G. Lada, Y. Sanakis, C. P. Raptopoulou, V. Psycharis, S. P. Perlepes, and G. Mitrikas, *Dalton Trans.*, 2017, **46**, 8458–8475.

77. M. Massacesi, G. Ponticelli, and V. G. Krishnan, *J. Mol. Struct.*, 1980, **69**, 165–181.

78. G. Tabbì, A. Giuffrida, and R. P. Bonomo, *J. Inorg. Biochem.*, 2013, **128**, 137–145.

79. X. Meng, X. Xu, T. Gao, and B. Chen, *Eur J. Org. Chem.*, 2010, **2010**, 5409–5414.

80. M. Morozova, M. S. Yusubov, B. Kratochvil, V. Eigner, A. Bondarev, A. Yoshimura, A. Saito, V. V. Zhdankin, M. E. Trusova, and P. S. Postnikov, *Org. Chem. Front.*, 2017, **4**, 1–77.

81. J. E. Leffler and R. D. Temple, *J. Am. Chem. Soc.*, 1967, **89**, 5235–5246.

82 B. T. Worell, J. A. Malik and V. V. Fokin, *Science*, 2013, **340**, 457-460.

83 F. Himo, T. Lovell, R. Hilgraf, V. V. Rostovtsev, L. Noodleman, K. B. Sharpless and V. V. Fokin, *J. Am. Chem. Soc.* 2005, **127**, 210–216.

Graphical Abstract

Copper(II)-benzotriazole coordination compounds in click chemistry: A diagnostic reactivity study

Edward Loukopoulos,[a] Alaa Abdul-Sada,[a] Gizella Csire,[b] Csilla Kállay,[c] Adam Brookfield,[d] Graham J. Tizzard,[e] Simon J. Coles,[e] Ioannis N. Lykakis*[f] and George E. Kostakis*[a]